Atmospheric Environment 180 (2018) 256–264

Contents lists available at ScienceDirect

Atmospheric Environment

journal homepage: www.elsevier.com/locate/atmosenv

SOA formation from photooxidation of naphthalene and methylnaphthalenes with *m*-xylene and surrogate mixtures

Chia-Li Chen[a,b,1], Lijie Li[a,b,2], Ping Tang[a,b], David R. Cocker III[a,b,*]

[a] Department of Chemical and Environmental Engineering, University of California, Riverside, CA, 92521, United States
[b] College of Engineering – Center for Environmental Research and Technology (CE-CERT), CA, 92507, United States

ARTICLE INFO

Keywords:
Secondary organic aerosol
m-Xylene
Polycyclic aromatic hydrocarbons
Two-product model
Surrogate mixture

ABSTRACT

SOA formation is not well predicted in current models in urban area. The interaction among multiple anthropogenic volatile organic compounds is essential for the SOA formation in the complex urban atmosphere. Secondary organic aerosol (SOA) from the photooxidation of naphthalene, 1-methylnaphthalene, and 2-methylnaphthalene as well as individual polycyclic aromatic hydrocarbons (PAHs) mixed with *m*-xylene or an atmospheric surrogate mixture was explored in the UCR CE-CERT environmental chamber under urban relevant low NO_x and extremely low NO_x (H_2O_2) conditions. Addition of *m*-xylene suppressed SOA formation from the individual PAH precursor. A similar suppression effect on SOA formation was observed during the surrogate mixture photooxidation suggesting the importance of gas-phase chemical reactivity to SOA formation. The SOA growth rate for different PAH-*m*-xylene mixtures was strongly correlated with initial $[HO_2]/[RO_2]$ ratio but negatively correlated with initial *m*-xylene/NO ratio. Decreasing SOA formation was observed for increasing *m*-xylene/PAHs ratios and increasing initial *m*-xylene/NO ratio. The SOA chemical composition characteristics such as f_{44} versus f_{43}, H/C ratio, O/C ratio, and the oxidation state of the carbon ($\overline{OS}_c$) were consistent with a continuously aging with the SOA exhibiting characteristics of both individual precursors. SOA formation from PAHs was also suppressed within an atmospheric surrogate mixture compared to the SOA formed from individual PAHs, indicating that atmospheric reactivity directly influences SOA formation from PAHs.

1. Introduction

Polycyclic aromatic hydrocarbons (PAHs) are significant components of semivolatile gas-phase emissions from anthropogenic sources including incomplete combustion emissions from heavy-duty diesel exhaust vehicles (Shah et al., 2005), biomass burning (Conde et al., 2005; Hedberg et al., 2002), and meat cooking (McDonald et al., 2003), and may be a major "missing" source of SOA. Formation of naphthalene and its alkyl derivatives are favored among PAHs and can represent as much as 80% of the total PAHs in a combustion smoke sample (Conde et al., 2005). Previous studies have shown that SOA yields for naphthalene, 1-methylnaphthalene, and 2-methylnaphthalene range from 0.04 to 1.81 (Chen et al., 2016; Shakya and Griffin, 2010; Nishino et al., 2012), which indicates a significant impact on SOA formation from anthropogenic sources.

Nitrogen oxides (NO_x) levels play an important role on SOA formation from small hydrocarbons (10 carbons or fewer)(Kroll et al., 2006; Ng et al., 2007; Song et al., 2005; Li et al., 2015). SOA yields are generally observed to decrease as NO_x increases; however, some studies observe reverse NO_x dependence at low NO_x level due to the formation of OH from NO (Kroll et al., 2006). RO_2· + NO and RO_2· + HO_2· oxidation mechanisms dominate the reaction pathway in forming volatile organic compounds (VOCs) oxidation products. *m*-Xylene has been extensively studied in smog chambers and significant SOA formation has been reported (e.g. (Bahreini et al., 2005; Chhabra et al., 2011; Cocker et al., 2001b; Izumi and Fukuyama, 1990; Li et al., 2015; Loza et al., 2012; Ng et al., 2007; Odum et al., 1996; Qi et al., 2010; Song et al., 2005, 2007; Takekawa et al., 2003; Nakao et al., 2011a; Sato et al., 2010). The chemical composition and aging properties of SOA formed from *m*-xylene photooxidation have been investigated previously; however, SOA formation from aromatic mixtures (e.g., with PAHs) is poorly understood. Previous chamber studies have reported that NO_x level influences SOA formation from *m*-xylene photooxidation—SOA formation per *m*-xylene reacted increases with decreasing NO_x levels (Li et al., 2015; Song et al., 2005). Song et al. (2007) studied SOA formation from *m*-xylene and utilized H_2O_2

* Corresponding author. Department of Chemical and Environmental Engineering, University of California, Riverside, CA, 92521, United States.
E-mail address: dcocker@engr.ucr.edu (D.R. Cocker).
[1] Currently at Scripps Institution of Oceanography, University of California, San Diego, La Jolla, CA, 92093, United States.
[2] Currently at Department of Environmental Science and Engineering, California Institute of Technology, CA, 91125, United States.

https://doi.org/10.1016/j.atmosenv.2018.02.051
Received 16 October 2017; Received in revised form 20 February 2018; Accepted 26 February 2018
Available online 02 March 2018
1352-2310/

photolysis as a hydroxyl radical source, leading to higher hydroxyl radical concentrations relative to NO_x experiments and thereby greater SOA formation. Hezne et al. (2008) reported that SOA yield increases when aromatic hydrocarbons react with OH instead of NO under lower [NO]/[HO_2] ratios. Therefore, gas phase radical conditions are significant factors to SOA formation from aromatic hydrocarbon precursors. The OH radical reactions occurred mainly by OH radical addition pathway (> 90%) to the aromatic ring(s) for both monocyclic aromatic hydrocarbons and PAHs (Atkinson and Arey, 2007; Li et al., 2017). Forstner et al. (1997) reported that major three products (approximately 75%) of SOA from *m*-xylene oxidation includes 3-methyl-2,5-furandione, *m*-toluic acid, and 2,5-furandione. For naphthalene SOA under low NO_x condition (with H_2O_2) ~26.2% is associated with organic peroxide compounds, and others are mainly from acids, such as hydroxyphthalic acid, 2-formylcinnamaldehyde (30–60%), phthaldialdehyde, phthalic anhydride (Atkinson and Arey, 2007; Nishino et al., 2012, 2009; Wang et al., 2007), and phthalic acid (Kautzman et al., 2010).

Previous studies reported that current climate and air quality models underestimate the total organic aerosols including primary organic aerosol (POA) and SOA in urban and remote areas (e.g. (Heald et al., 2005; Volkamer et al., 2006; Kleinman et al., 2008; Utembe et al., 2011; Hodzic et al., 2009; Henze et al., 2008). It is hypothesized that the underestimation is attributable to missing chemical reaction processes and errors in SOA photochemical (Zhang et al., 2006) as well as overestimation of POA (de Gouw et al., 2005). Hodzic et al. (2009) reported that anthropogenic SOA is underestimated by a factor of two in the late morning with the discrepancy increasing rapidly during the day. Volkamer et al. (2006) also estimated that anthropogenic SOA is underestimated by a factor of 5 after especially when photochemistry enhance an order magnitude after few hours of photooxidation.

Currently, SOA formation potentials are measured from single precursors where the atmospheric reactivity of the chamber study is set by the individual oxidizing species and NO_x/oxidants injected. However, these precursors react in a complex atmospheric mixture dictated by atmospheric NO_x and many other volatile organic compounds present especially in the urban atmosphere. Therefore, this study investigates how the individual SOA formation from select PAHs is influenced by the presence of other VOCs. This study takes advantage of the extensive *m*-xylene experimental database and previous studies to identify how a simple VOC mixture impacts SOA formation from PAH precursors. Further, the atmospheric reactivity is controlled by an atmospheric surrogate developed by Carter (2010) to explore the impact of atmospheric reactivity on SOA formation from individual PAH.

2. Experimental methodology

2.1. Experimental setup

All mixtures and individual PAH experiments were conducted in the UCR/CE-CERT environmental chamber described in detail elsewhere (Carter et al., 2005). The facility includes a 6 m × 6 m × 12 m thermally insulated enclosure, which is continuously flushed with purified air (Aadco 737 series (Cleves, Ohio) air purification system). Inside the enclosure, there are two 90 m^3 2 mil (54 μm) FEP Teflon® film reactors, and four banks of 115 W 4-ft blacklights for driving NO_2 photolysis within the reactor. The top frames of the chamber are controlled by elevators that maintain a positive differential pressure of ~0.02" H_2O. Aliquots of volatile organic compound were injected into the chamber through a heated glass injection manifold system and flushed into the chamber with pure N_2. PAHs and hydrogen peroxide (50 wt% H_2O_2) were injected into a glass manifold tube with a 55 °C oven, and flushed into the chamber with purified air. NO was prepared by filling a calibrated glass bulb to a known pressure of pure NO followed by flushing into the chamber with pure N_2. The full surrogate used for select experiments consists of *n*-butane (135 ppb), *n*-octane (36 ppb), ethane (25 ppb), propene (20 ppb), *trans*-2-butene (20 ppb), toluene (33 ppb), and *m*-xylene (31 ppb) (Carter, 2010). 100 ppb perfluorohexane was injected into the chamber as an inert tracer.

2.2. Instrumentation

Gas phase: Hydrocarbon decay and perfluorohexane were monitored with dual Agilent 6 980 (Palo Alto, CA) gas chromatographs (GC) equipped with flame ionization detectors (FIDs). NO and NO_x were measured by a TECO model 42 chemiluminescence NO_x analyzer while O_3 was monitored with a Dasibi Environmental Corp. Model 1 003-AH O_3 analyzer.

Particle phase: Particle size distributions (27–686 nm) and number concentrations were measured with an in-house build Scanning Mobility Particle Sizers (SMPS) described by Cocker et al. (2001a). Aerosol particle density was measured with an aerosol particle mass analyzer (APM, Kanomax model 3 600) and SMPS in series (APM-SMPS). A detailed description of APM-SMPS is described elsewhere (Malloy et al., 2009; Nakao et al., 2011b). Particle volatility was monitored with a volatility tandem differential mobility analyzer (VTDMA) (Nakao et al., 2012) for which monodisperse particles of mobility diameter (D_{mi}) are selected by the 1st differential mobility analyzer (DMA) followed by transport through a Dekati thermodenuder (TD, residence time: ~16 s, at 100 °C) and resizing after the TD in the second DMA column (D_{mf}). Volume remaining fraction (VRF) is then calculated as VRF = $(D_{mf}/D_{mi})^3$.

High-Resolution Time-of-Flight Aerosol Mass Spectrometer (HR-ToF-AMS) has been widely used to provide quantitative chemical composition and size-resolved mass distributions with high time resolution (Aiken et al., 2007, 2008; DeCarlo et al., 2006). Details of the HR-ToF-AMS and software analysis are described in DeCarlo et al. (2006). This study used W-mode for higher mass resolution analysis, including *mass-to-charge* (*m/z*) distribution, elementary analysis of elemental carbon (EC) and organic carbon (OC). Data was analyzed with ToF-AMS analysis toolkit squirrel 1.56D/PIKA 1.15D version.

2.3. Gas-phase kinetic modeling of radical species

The OH radical concentration was estimated by fitting the *m*-xylene decays, using the SAPRC gas-phase mechanism (Carter and Heo, 2013). SAPRC 12 was then used to estimate HO_2 and RO_2 radical concentration. Further, the model used a kinetic and equilibrium approach to predict secondary particulate matter formation and ozone (Carter, 2010; Carter and Heo, 2013).

2.4. SOA yield

SOA formation is evaluated assuming gas-particle partitioning equilibrium of semivolatile partitioning products is achieved. Odum et al. (1996, 1997) established the expression of fractional SOA yield (Y) to describe the gas-particle partitioning absorption model. SOA yield for individual hydrocarbons is defined by equation (1), where ΔM_o (μg m^{-3}) is the total organic aerosol mass concentration, ΔHC (μg m^{-3}) is the amount of hydrocarbon reacted, and α_i and $K_{om,i}$ (m^3 μg^{-1}) are the mass-based stoichiometric coefficient and absorption equilibrium partitioning coefficient of product *i*, respectively.

$$Y = \frac{\Delta M_o}{\Delta HC} = \sum_i^n Y_i = M_o \sum_{i=1}^n \frac{\alpha_i K_{om,i}}{1 + K_{om,i} M_o} \quad (1)$$

Total organic aerosol formation for multicomponent mixture is estimated from individual VOC yields by:

$$M_{o\ total\ estimated} = \sum Y_{HC,i}\, \Delta HC_{HC,i} \quad (2)$$

$$M_{o\ predicted} = Y_{HC,1} \times \Delta HC_{HC,1} + Y_{HC,2} \times \Delta HC_{HC,2} \quad (3)$$

Table 1
Initial experimental conditions and SOA yields for all experiments.

Run number	Compounds	Initial PAHs	Initial *m*-xylene	ΔHC_PAHs	ΔHC_ *m*-xylene	NO[e]	ΔM_o	SOA yield	Density
		ppb	ppb	μg m^{-3}	μg m^{-3}	ppb	μg m^{-3}		g cm^{-3}
1784A	naphthalene + *m*-xylene	36.6	114.8	124.3	247.9	12.5	42.0	0.11	1.37
1784B	naphthalene	37.7	–	184.7	–	12.4	39.7	0.21	a
1788A	naphthalene + *m*-xylene	68.6	44.9	209.3	92.2	8.3	61.7	0.20	1.33
1788B	*m*-xylene	–	44.0	–	158.5	8.1	4.8	0.03	b
1791A	naphthalene + *m*-xylene	32.1	94.4	106.8	187.4	8.7	39.4	0.13	1.33
1791B	*m*-xylene	–	91.8	–	248.1	8.7	7.2	0.03	b
1794A	naphthalene + *m*-xylene	49.5	50.0	181.9	117.1	9.5	55.0	0.18	1.34
1794B	naphthalene	50.9	–	226.1	–	9.5	79.9	0.35	a
1797A	naphthalene + *m*-xylene	53.5	50.9	184.8	145.7	11.5	71.3	0.22	1.32
1797B	*m*-xylene	–	58.9	–	201.0	11.5	11.6	0.06	b
1800A	naphthalene + *m*-xylene	30.0	111.2	102.9	242.1	12.2	40.9	0.12	1.33
1800B	naphthalene	29.8	–	148.6	–	12.1	47.8	0.32	a
1959A	naphthalene + *m*-xylene	34.1	110.0	118.8	185.2	12.4	50.3	0.17	1.42
1959B	naphthalene	34.1		156.6	–	12.5	79.0	0.50	a
1804A	1-methylnaphthalene + *m*-xylene	38.2	125.3	152.8	214.0	12.4	123.9	0.34	1.30
1804B	1-methylnaphthalene	38.8	–	203.9	–	12.1	136.3	0.67	c
1805A	1-methylnaphthalene + *m*-xylene	66.5	66.7	227.8	115.9	12.7	155.3	0.45	1.33
1805B	1-methylnaphthalene	65.9	–	303.7	–	12.5	152.8	0.50	c
1808A	1-methylnaphthalene + *m*-xylene	32.8	129.4	122.7	193.0	11.8	81.9	0.26	1.31
1808B	1-methylnaphthalene	34.8	–	176.0	–	11.8	95.1	0.54	c
1976A	1-methylnaphthalene + *m*-xylene	36.5	120.5	161.7	215.1	10.7	137.3	0.36	1.35
1976B	1-methylnaphthalene	38.5	–	214.9	–	11.0	158.8	0.74	c
1978A	1-methylnaphthalene	25.9	–	130.9	–	11.5	112.4	0.86	1.48
1978B	1-methylnaphthalene + *m*-xylene	28.2	68.8	128.1	136.3	11.5	137.5	0.52	
1936A	2-methylnaphthalene + *m*-xylene	36.1	117.8	158.2	234.8	11.5	58.2	0.15	1.37
1936B	2-methylnaphthalene	35.5	–	213.5	–	11.4	84.2	0.39	d
1979A	2-methylnaphthalene + *m*-xylene	48.8	61.3	236.4	134.6	12.6	131.8	0.36	1.38
1979B	2-methylnaphthalene	54.5	–	301.0	–	12.5	151.9	0.50	d
1981A	2-methylnaphthalene + *m*-xylene	26.0	117.0	119.8	226.1	12.4	78.4	0.23	1.35
1981B	2-methylnaphthalene	28.2	–	160.5	–	12.4	134.8	0.84	d
1982A	2-methylnaphthalene	39.0	–	216.0	–	13.0	108.0	0.50	1.44
1982B	2-methylnaphthalene + *m*-xylene	36.9	69.2	188.5	161.6	12.9	103.5	0.30	d

[a], [b], [c], and [d]: The experiment lacks the measurement of density, so the assumed density is derived from the average of individual PAH or *m*-xylene experiments. [a]: Assumed density for naphthalene is 1.48 g cm^{-3}; [b]: Assumed density for *m*-xylene is 1.4 g cm^{-3}[c]: Assumed density for 1-methylnaphthalene is 1.41 g cm^{-3}; [d]: Assumed density for 2-methylnaphthalene is 1.37 g cm^{-3} [e]: In the absence of H_2O_2.

where $Y_{HC,i}$ is estimated from the α_i and $K_{om,i}$ in (eq (1)) and total aerosol mass concentration measured. In this study, $Y_{m\text{-xylene\_predicted}}$ and $Y_{naphthalene\_predicted}$ is defined as following equations:

$$Y_{m-xylene,predicted} = \frac{M_{o\ m-xylene,predicted}}{\Delta\ HC_{m-xylene}} \quad (4)$$

$$Y_{naphthalene,predicted} = \frac{M_{o\ naphthalene,predicted}}{\Delta\ HC_{naphthalene}} \quad (5)$$

3. Results and discussion

3.1. SOA formation from mixtures of m-xylene and individual PAH

All experiments were conducted for 6–8 h at UCR CE-CERT environmental chamber at T = 27 °C and RH < 0.1%. Table 1 summarizes the key parameters of SOA experiments along with total organic aerosol mass formed, SOA yields, and average density. Empirical fits to the two-product model (eq (1)) for naphthalene, 1-methylnaphthalene, and 2-methylnaphthalene under various conditions have been explored previously within the same chamber under the same light, RH, and temperature conditions (Table S1) (Chen et al., 2016). Fig. S1 shows the two-product model curves for three individual PAH under different conditions including H_2O_2 with NO and without NO addition (curve1), high NO_x + HONO (curve 2), low NO_x (curve 3), along with *m*-xylene SOA yield curves obtained for similar conditions (Song et al., 2005). The two-product model SOA yield curve 3 for low NO_x condition and curve 1 for H_2O_2 condition were used in this study for predicting the total organic aerosol formation for individual PAH and *m*-xylene. The predicted to measured organic aerosol mass concentration (M_o) for mixtures of individual PAH with *m*-xylene are summarized (Table S2). $Y_{predicted}/Y_{measured}$ ranges from 1.23 to 1.61, 0.78–1.15, and 1.08–1.59 for *m*-xylene/naphthalene mixture, *m*-xylene/1-methylnaphthalene, and *m*-xylene/2-methylnaphthalene, respectively for low NO_x conditions. Measured versus predicted SOA formation for each PAH/*m*-xylene photooxidation experiment (Fig. 1) shows a linear correlation with a 0.90 (~10% less SOA is formed than prediction). *m*-Xylene/1-methylnaphthalene produced a higher SOA yield than *m*-xylene with 2-methylnaphthalene or naphthalene, consistent with individual PAH photooxidation SOA yield (Chen et al., 2016). SOA formation from PAH and *m*-xylene mixtures are expected to be affected by the initial PAHs/NO ratio, *m*-xylene/NO ratio, *m*-xylene/PAHs mixing ratio and other changes to the reactivity of the system. The VOCs/NO ratio has previously been found to affect the SOA formation from aromatic precursors (Li et al., 2015, 2016; Song et al., 2005) by influencing the relative abundance of radicals (e.g., RO_2:HO_2:OH) in the system. Therefore, differences between reactivity from individual precursor/NO_x system and those induced by addition of different hydrocarbons changes the aerosol formation estimated by using the simple gas-particle partitioning approach where the hydrocarbon mixture aerosol formation is predicted from the sum of individual precursors. The two-product model for this particular matter over predicts the experimentally observed SOA formation. The bias increases might result from increasing *m*-xylene/PAH ratio. The bias may be induced by changes to the reactivity of the overall system (e.g., HO_2/HO ratios, OH concentration, HO_2/NO or RO_2/NO ratio, etc.) or by additional cross-reaction between oxidation products from the two individual precursors. A previous study observed cross-reactions of glyoxal and methylglyoxal

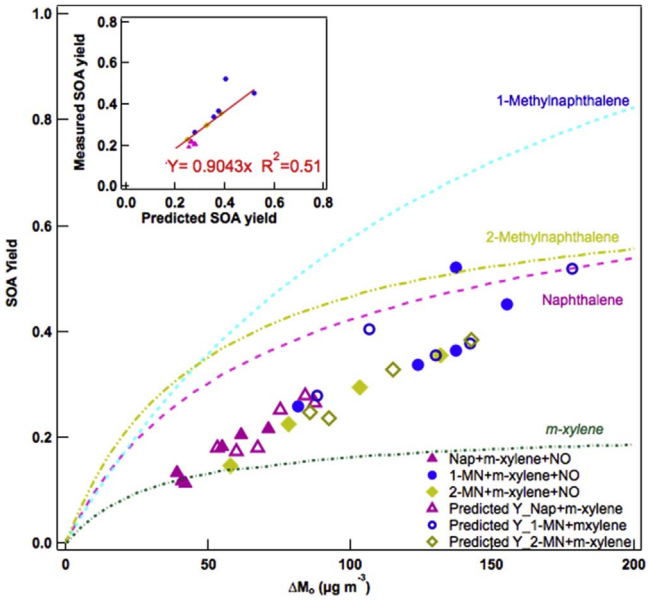

Fig. 1. Secondary organic aerosol yields as a function of organic aerosol mass concentration (ΔM_o) for each PAH/*m*-xylene mixture experiment under low NO_x condition. Left upper figure represents the linear relationship of measured SOA yields and predicted SOA yields. Dashed curves are derived from each PAH curve 3 as shown in Fig. S1.

during secondary organic aerosol formation (Schwier et al., 2010). Section 3.7 addresses the significance of cross-reaction between oxidation products from mixture precursors.

The relationship between SOA yield and the initial *m*-xylene/PAHs (0.7–3.7) is shown in Fig. 2. Initial PAH hydrocarbon concentration at low NO_x conditions is the key metric for estimating the SOA formation from aromatic/PAH hydrocarbon photooxidation. $Y_{m\text{-xylene predicted}}$ is constant with initial *m*-xylene/PAHs since the SOA yield for *m*-xylene is located on the plateau of two-product curve for the given aerosol mass concentration. The SOA yield for naphthalene prediction ($Y_{naphthalene\ predicted}$) decreases from 0.34 to 0.26, indicating *m*-xylene addition suppresses naphthalene SOA yield. Overall, the total SOA yield (Y_{total}) and total M_o decrease as the initial *m*-xylene/PAHs increases. The $M_{o\_predicted}$ is higher than the $M_{o\_measured}$ for naphthalene/*m*-xylene mixture by 23%–61% and is not a function of total ΔHC (Fig. S2). This study suggests additional precursor *m*-xylene suppressed the SOA formation from naphthalene.

3.2. Overall and instantaneous aerosol formation after onset of aerosol growth

The timing for the onset of new particle formation was identified as the time at which aerosol mass concentration (ΔM_o) equaled 2 μg m^{-3}. Aerosol yield can then be estimated as the amount growth after the new particle induction period versus the hydrocarbon consumed after new particle formation commences (Li et al., 2015). The onset of new particle formation varies widely—for example, exp. 1784A (naphthalene 36.6 ppb, *m*-xylene 114.8 ppb, NO 12.5 ppb) has an irradiation of 41 min while exp. 1784B (naphthalene 37.7 ppb, no *m*-xylene, NO 12.4 ppb) has an irradiation time of 156 min (Fig. S3 and Table S3). Fig. 3 compares aerosol growth with and without shifting for timing of new particle formation. The aerosol growth curve is almost linear after offset with linear regression for each system. The slope of the line then indicates the aerosol yield accounting only for hydrocarbon decay after the onset of aerosol formation. This implies three important observations: 1) aerosol formation is independent of the HC consumed prior to aerosol formation; 2) the aerosol formation after particle formation is not strongly influenced by organic aerosol mass concentration present for these mixture systems; and 3) addition of species that influence the timing of aerosol formation by altering the reactivity of the system will directly impact total aerosol formation; therefore **Δ**HC precursor reacted after the onset of aerosol formation.

The higher the initial *m*-xylene/naphthalene ratio the lower the slope is consistent with the lower SOA yield under higher *m*-xylene/naphthalene ratio. *m*-Xylene decay is observed (Table S3 and Fig. S3) to be faster than naphthalene when the initial *m*-xylene to naphthalene (ppbv/ppbv) mixing ratio is greater than 1 (e.g., 1784A, 1791A, and 1800A). Conversely, for mixing ratios less than 1 the naphthalene is observed to decay faster than the *m*-xylene (Table S3). This indicates that the addition of mixture species changing the time of **Δ**HC precursor reacted. Therefore, the initial hydrocarbon mixing ratio is a critical factor to determine the contribution of different precursor to SOA formation for constant NO range.

Aerosol mass concentration starts to increase for the *m*-xylene/naphthalene mixture experiment, only after the NO decreases from 12.5 ppb to 1 ppb (t = 33 min) (Fig. S4). The irradiation time for NO to consume to sub-ppb level from naphthalene without *m*-xylene is much

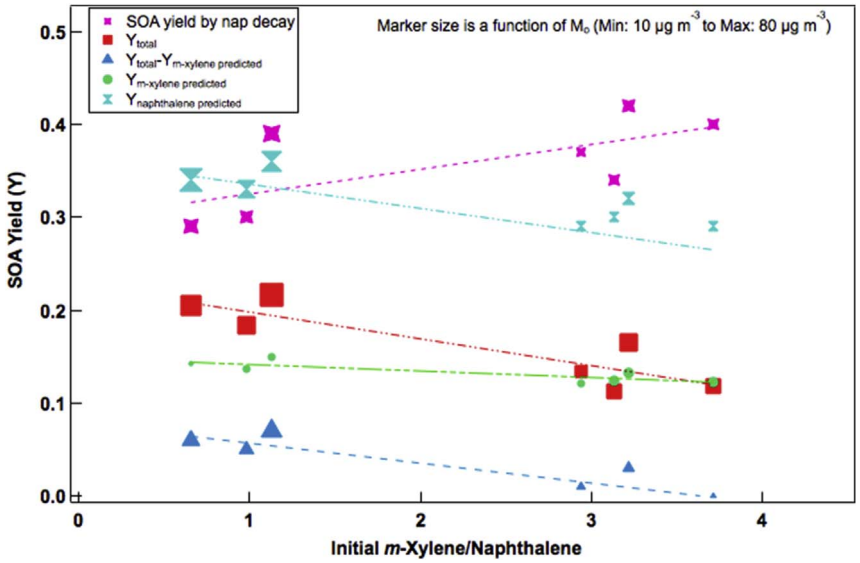

Fig. 2. Relationship between initial *m*-xylene/naphthalene and SOA yield. Marker size is a function of M_o (from 10 μg m^{-3} to 80 μg m^{-3}). "SOA yield by nap decay" represents SOA yield is estimated by total organic aerosol divided by naphthalene decay only.

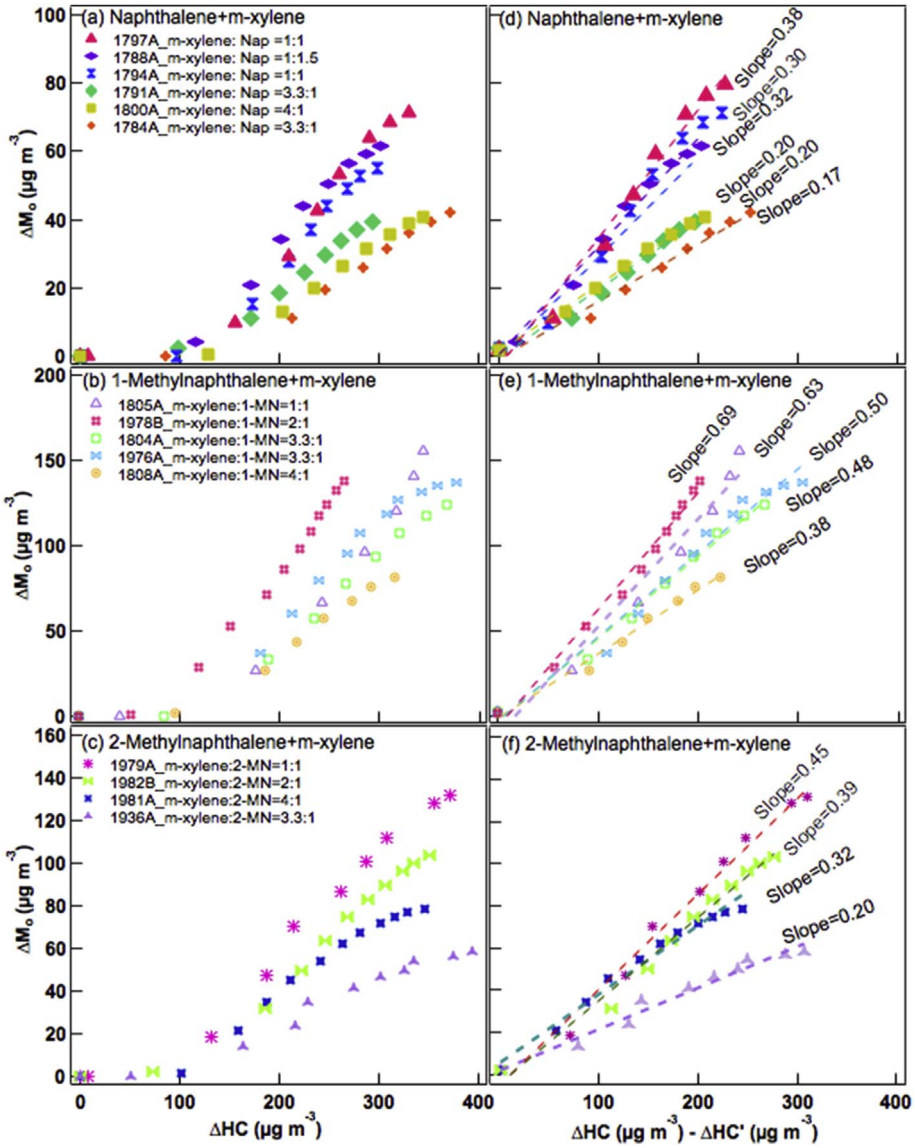

Fig. 3. SOA mass concentration (ΔM_o) from (a) naphthalene/*m*-xylene, (b) 1-methylnaphthalene/*m*-xylene, and (c) 2-methylnaphthalene/*m*-xylene mixture photooxidation experiments as a function of total hydrocarbon consumption (ΔHC). Right panels represent the liner relationship of SOA mass concentration with the difference of total hydrocarbon reacted with the first hydrocarbon decay at the initial lag phase (ΔHC- ΔHC′) for (d) naphthalene/*m*-xylene, (e) 1-methylnaphthalene/*m*-xylene, and (f) 2-methylnaphthalene/*m*-xylene mixture photooxidation experiments. ΔHC′ represents the first hydrocarbon decay at the initial lag phase.

longer than the mixture (188 min). SAPRC-12 gas-phase chemical model predicts RO_2 and HO_2 radicals to sharply increase to 10^9 molecules cm^{-3} level when NO is depleted (Fig. S5). Competition for available hydroxyl radical led to the consumption of only 50% and 65% of the precursor *m*-xylene and naphthalene, respectively versus 94% naphthalene consumption in the naphthalene-NO_x experiment. The mixture experiment's rapid conversion of NO to NO_2 greatly enhanced HO_2+RO_2 reaction while the slow conversion of NO to NO_2 in naphthalene experiment led to greater contribution of RO_2+NO chemistry. Therefore, it is expected that the mixture experiment will lead to lower volatility hydroperoxides products (ROOH) compared with the reactivity higher volatility RO_2+NO products (e.g., nitronaphthalene, and naphthoquinone (Kautzman et al., 2010)).

3.3. SOA growth rate for different PAH mixtures

SOA mass concentration (ΔM_o) as a function of total hydrocarbon reacted for *m*-xylene/PAH photooxidation experiments was shown for different mixing ratio all with similar initial NO levels (Fig. 3a, b, and 3c). The hydrocarbon reacted lag phase (ΔHC′, the hydrocarbon reacted when $\Delta M_o \geq 2\,\mu g\,m^{-3}$) was subtracted from total HC reacted (ΔHC) (Fig. 3d, e, and 3f). The relationship of M_o and ΔHC − ΔHC' was linearly curve fit with the slope representing the SOA formation rate for each experiment after onset of particle growth. The slopes are the highest (0.38 and 0.45) when the mixing ratio is 1:1 for naphthalene and 2-methylnaphthalene, respectively, but the slope is the highest when the mixing ratio is 2:1 for 2-methylnaphthalene, likely due to the different reaction mechanism. The SOA formation growth rate was explored for different *m*-xylene/PAH mixtures by investigating the correlations with OH radical, HO_2, RO_2 radical, and the different mixing ratios (Fig. 4 and Table S4). The relationship of SOA formation rate to average OH concentration (Fig. 4a) suggests that the OH radical alone concentration is not the determining factor for aerosol production in the naphthalene/*m*-xylene mixture photooxidation. Only using OH radical concentration cannot explain the gas phase reactivity. Integrated $[OH]/[HO_2]$ ratio (Fig. 4b) ranges from 1.03×10^{-3} to 6.43×10^{-3} for the various mixtures with SOA growth rate slightly increasing with increasing $[OH]/[HO_2]$ ratio. Furthermore, if we consider $[NO]/[HO_2]$ (Fig. 4c),

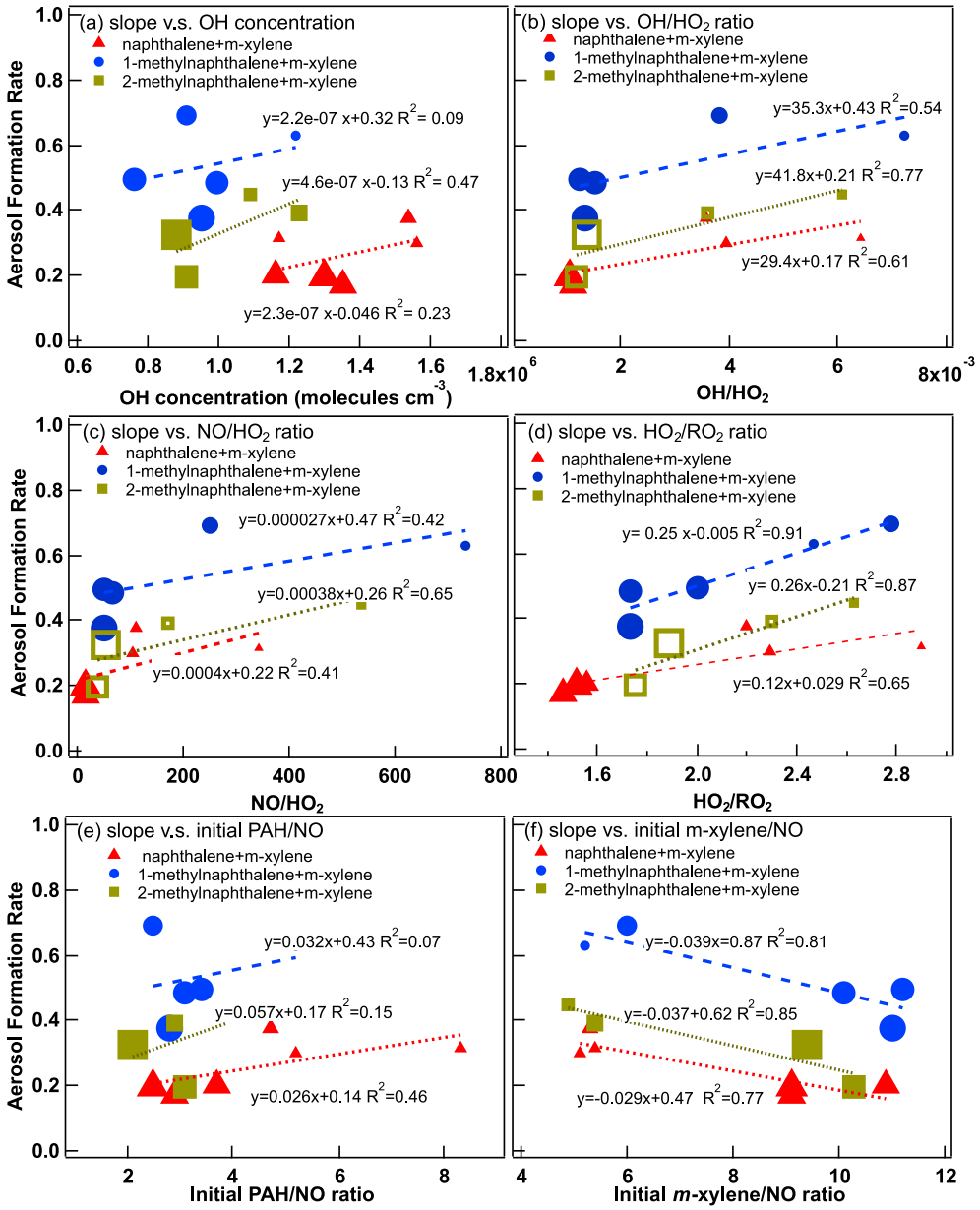

Fig. 4. SOA formation rate of PAH/*m*-xylene mixture hydrocarbon reacted after the lag phase versus with (a) the [OH] radical concentration; (b) [OH]/[HO_2] ratio; (c) [NO]/[HO_2] ratio; (d) [HO_2]/[RO_2] ratio; (e) initial PAH/NO ratio; (f) initial *m*-xylene/NO ratio. Marker size as a function of initial *m*-xylene/PAH concentration (min:0 ~max: 5). In this study we consider r^2 between 0.64 and 1.0 ($0.8 \leq |r| \leq 1$) to be a strong correlation, r^2 less than 0.25 ($0 \leq |r| \leq 0.5$) to be weak, and otherwise to be moderate (Devore and Berk, 2012).

the SOA growth rate is observed to increase with [NO]/[HO_2] ratio. The [NO]/[HO_2] trend is opposite of that suggested by Henze et al. (2008). They suggest based on global modeling that aromatic species produce more SOA when they react with OH radicals in regions where the [NO]/[HO_2] ratios are lower. A strong positive correlation between SOA formation and [HO_2]/[RO_2] ratios was observed (Fig. 4d), suggesting increasing $HO_2 + RO_2$ chemistry enhances SOA formation. High initial PAH/NO ratio (Fig. 4e) and the low initial *m*-xylene/NO ratio (Fig. 4f) are also weakly associated with more SOA formation, suggesting *m*-xylene inhibits OH radical availability for PAH reaction in the PAH/*m*-xylene low NO_x condition. However, the limitation and uncertainties of these results from Fig. 4 include the limited experimental data available for PAH/*m*-xylene mixtures, and the uncertainties of the SAPRC model predicting HO_2 and RO_2. The uncertainties in radical estimates may originate from uncertainties in the SAPRC model estimated mechanism and relevant rate constant(s) or photolysis rates; however, other applications of mechanisms based on similar assumptions have been found to perform reasonably for related compounds (Carter, 2010).

The individual PAHs have a delayed second step oxidation relative to first step oxidation aerosol growth evidenced by a "hook" (also observed in Chan et al., 2009) at the end of higher hydrocarbon reacted (ΔHC) (Fig. S6); the mixtures lack the "hook" suggesting different chemical pathways for individual PAHs and mixtures. The SOA formation from 1-methylnaphthalene is observed to be higher (Fig. 4) than naphthalene or 2-methylnapthalene. This is consistent with earlier studies suggesting that the mechanism of OH radical oxidation for 1-methylnaphthalene is different than naphthalene and 2-methylnaphthalene. The OH addition most frequently occurs at the C2 position for 1-methylnaphthalene, while the OH addition most frequently occurs at C1 position for naphthalene and 2-methylnaphthalene (Wang et al., 2007; Kautzman et al., 2010). More aldehyde group compounds formed from oxidation of first-generation dicarbonyl fragment product from 2-methylnaphthalene photooxidation than 1-methylnaphthalene (Chen

et al., 2016).

3.4. Mixtures under absence of NO_x

Song et al. (2007) observed that SOA mass concentration from aromatics is enhanced by injecting H_2O_2 as it increases hydroxyl radical levels which in turn increase organic peroxide formation rates. SOA yields from PAH precursors were suppressed as more *m*-xylene was added, consistent with observations from the low NO_x condition (Table S4). The two-product model overestimates aerosol formation for *m*-xylene/naphthalene photooxidation by 34%–78% based on individual PAH/H_2O_2 and *m*-xylene/H_2O_2 two-product model curves (as Table S1 and Fig. S7). Adding *m*-xylene to PAHs photooxidation reduces the OH radicals for all PAH/*m*-xylene mixtures H_2O_2 experiments (Fig. S8) and SOA formation from the precursors. Therefore, the overprediction of SOA formation from the two-product model derives from changes to the OH radical levels by the mixture of precursors versus of the individual precursor.

3.5. Individual PAH/surrogate mixture

An ambient surrogate mixture (Carter, 2010) was introduced into the PAH system to further understand the effect of mixture compounds in the atmosphere. The initial condition and experimental results for individual PAH and surrogate mixture photooxidation experiments in the absence and presence of NO_x are summarized (Table S5). The H_2O_2 (runs: 1814AB) was injected as an additional OH radical source, thereby increasing both OH and hydroperoxyl (HO_2) radicals. CO was introduced with H_2O_2 (run: 1814A) to further promote HO_2 radical concentration through the CO oxidation cycle. SOA formation from the naphthalene/surrogate is less than 5 μg m^{-3} with addition of CO and H_2O_2 condition (run: 1814A), while the experiment without CO addition formed more aerosol mass concentration (73.1 μg m^{-3}, run: 1814B) (Fig. S9). The large differences in aerosol formation are attributed to greatly reduced OH superceding any additional aerosol formation through increasing HO_2. The HO_2 radical increases rapidly at the onset of aerosol formation (Fig. S9), which indicates that the CO and surrogate reacted with OH radical and formed more HO_2 as well as lower PAH reacted leading to lower SOA formation. The surrogate mixture in the presence of NO_x inhibits SOA formation from individual PAH photooxidation, indicating that SOA formation from PAH is less pronounced due to the atmospheric reactivity conditions changed by the addition of the ambient surrogate. Some intermediate species from the surrogate mixture system could influence SOA formation by changing OH radical concentrations and the volatility of condensable species (e.g., glyoxal uptake on SOA from toluene photooxidation under NO_x condition (Nakao et al., 2012).) Similarly, the presence of the surrogate mixture during photooxidation of intermediate-low volatility organic compounds from consumer products was also found to influence SOA and O_3 formation (Li et al., 2018).

3.6. Volatility and density evolution

Volume remaining fraction (VRF) evolution of SOA generated from different *m*-xylene/PAHs mixtures photooxidation is shown in Fig. S10 and Table S6. VRF increased from 0.26 to 0.69 for the 1:1.5 (*m*-xylene:naphthalene) mixing ratio. Previously, our group reported the VRF increasing from 0.35 to 0.7 for naphthalene/low NO_x experiment (Chen et al., 2016) and from 0.21 to 0.4 for *m*-xylene/low NO_x experiment (Li et al., 2015). Therefore, the mixture VRF of 0.69 is indicative of low volatility aerosol mainly from naphthalene photooxidation. Increasing the mixing ratio (*m*-xylene:PAH) from 1:1 to 4:1 decreased the final VRF from 0.66 to 0.55, 0.74 to 0.65, and 0.70 to 0.56, respectively for *m*-xylene mixtures with naphthalene, 1-methylnaphthalene, 2-methylnaphthalene, indicating *m*-xylene addition increases the volatility of secondary organic products. The 1-methylnapthalene/*m*-xylene mixture formed the lowest volatility products, consistent with the VRF order from individual PAH (Chen et al., 2016).

Densities for each *m*-xylene/PAHs mixture experiment (Table 1) and density evolution (Fig. S11) are provided for low NO_x conditions. The average density ranges from 1.32 to 1.42 for *m*-xylene/naphthalene mixture, from 1.30 to 1.40 for *m*-xylene/1-methylnaphthalene mixture, and from 1.35 to 1.37 for *m*-xylene/2-methylnaphthalene mixture. No obvious changes in density occur as each PAH/*m*-xylene experiment progresses (Fig. S11).

3.7. Chemical composition of PAHs mixtures

3.7.1. Cross-reaction effect evaluation

This study evaluated the cross-reaction effect by two methods—the unique *m/z* indicator mass-balance approach and the two-product model. Three representative average spectral distributions of 2-methylnaphthalene, *m*-xylene and 2-methylnaphthalene + *m*-xylene are shown (Fig. S12). The *m/z* 43 and *m/z* 44 are the two dominant fragments from *m*-xylene and 2-methylnaphthalene photooxidation. The *m/z* 43 ($C_2H_3O^+$ or $C_3H_7^+$) indicates oxidized organic compounds such as aldehydes and ketones (CH_2CHO^+ or CH_3CO^+) and saturated hydrocarbon compounds ($C_3H_7^+$)(Alfarra et al., 2004). The mass spectrum distribution from the *m*-xylene/2-methylnaphthalene mixture combines fragments from individual 2-methylnaphthalene and *m*-xylene photooxidation experiments with the higher *m/z* fragment (*m/z* > 100) is dominated by PAHs. To explore the relative SOA production from each mixture components, and from cross reaction, the unique *m/z* indicators were chosen and analyzed by a mass-balance approach:

$$(M_o\ contribution\ of\ m-xylene\ to\ AMS\ signal\ of\ mixed\ exp.) + (M_o\ contribution\ of\ PAHs\ to\ AMS\ signal\ of\ mixed\ exp.) + M_o cross\ reaction = total\ M_o \quad (6)$$

$$\frac{mix.\ exp.\ signal(\sum i)}{\frac{\sum i}{M_0\_m-xylene\ only}} + \frac{mix.\ exp.\ signal(\sum i)}{\frac{\sum i}{M_0\_PAHs\ only}} + M_{0\_cross\ reaction} = total\ M_0 \quad (7)$$

where M_o is total organic aerosol mass concentration (μg m^{-3}), and $\sum i$ are the unique *m/z* indicators for each individual *m*-xylene or PAHs. In this study, *m*-xylene has unique *m/z* at 95 ($C_7H_{11}^+$ or $C_6H_7O^+$), which is a fragment in individual *m*-xylene SOA but not a observed unique fragment in individual PAH; and naphthalene has unique *m/z* at 76, 104, 105; 1-methylnaphthalene has unique *m/z* at 76, 104, 105, 115, and 147; and 2-methylnapthalene has unique *m/z* at 76, 104, 105, 115, and 147. The $M_{o\ cross\text{-}reaction}$ was calculated by equations (6) and (7) based on individual *m*-xylene (1193A and 1930A) and PAH experiments (Table S7). The aerosol mass concentration $M_{o\ cross\text{-}reaction}$ is from 0.65 to −9.66 μg m^{-3} for *m*-xylene/naphthalene mixture experiment, suggesting little to no effect of cross-reaction between naphthalene and *m*-xylene precursors. However, since the *m/z* 95 is a minor *m*-xylene SOA fragment, significant discrepancies are observed from each individual experiment. Therefore, the M_o contribution prediction from two-product model is compared with the AMS evaluation method (Table S7). The two-product model prediction of the individual contribution to aerosol mass concentration is more plausible; the AMS method has great uncertainties associated with unique *m/z* fragments leading to the significant percentage discrepancy in estimates of individual contributors between experiments.

3.7.2. Triangle plot and Van Krevelen diagram analysis

m-Xylene/PAHs photooxidation experiments were evaluated with two common AMS analyses (“ Triangle plot” (Ng et al., 2010) and “Van Krevelen diagram” (Heald et al., 2010) (Fig. S13). All SOA from three *m*-xylene/PAHs mixtures lies on the lower side of triangle area indicating these SOA mixtures are semivolatile oxygenated organic

aerosol (SV-OOA). Chen et al. (2016) investigated each individual PAH (naphthalene, 1-methylnaphthalene, and 2-methylnaphthalene) SOA, all of which are located on the upper side of triangle area. Previous studies reported that SOA continuously ages (higher fragment m/z 44 (CO_2^+) intensity) with 33% organic acid SOA from low NO_x with H_2O_2 naphthalene photooxidation (Chhabra et al., 2010; Kautzman et al., 2010). This study observes that SOA from *m*-xylene/PAHs mixtures age with increasing f_{44} and f_{43}. Elevated m/z 44 (CO_2^+) is considered "aged" organic aerosol and classified as low volatility oxygenated organic aerosol (LV-OOA) while SV-OOA is associated with "fresh" OOA with elevated m/z 43 ($C_2H_3O^+$) signal intensity (Chhabra et al., 2011). The m/z 44 (CO_2^+) fragment is associated with thermal decarboxylation of many different oxo-, di-, and poly carboxylic acids, hydroxyl-acids, and acyl peroxides (Aiken et al., 2007; Alfarra et al., 2004; Duplissy et al., 2011; Zhang et al., 2007). Recent studies (Li et al., 2016; Loza et al., 2012) have reported that *m*-xylene SOA lies on the right of the triangle region with f_{43} higher than the ambient SOA reported by Ng et al. (2010).

Previous studies have observed that atmospheric organic aerosol lies on the −1 slope of Van Krevelen diagram (H:C versus O:C). Heald et al. (2010) suggested that the slope is the addition of carboxylic acid or equal addition of hydroxyl and carbonyl functional groups to an aliphatic (unfunctionalized) carbon. *m*-Xylene/PAHs mixtures in this study occupy the area between a slope of −1 and −2 on Van Krevelen diagram (Fig. S13 (b)). The slope of −1 for naphthalene and 2-methylnaphthalene indicates greater addition of carboxylic acid groups to the precursor. However, the *m*-xylene/1-methylnaphthalene mixture SOA lies on the area with slope −2, which indicates less formation of carboxylic acid and more ketone/aldehyde functionality to the precursor molecule.

Furthermore, SOA with higher f_{44} increases O/C values and the state of the carbon ($\overline{OS}_c$) (Kroll et al., 2011; Ng et al., 2010). The simplified equation describing $\overline{OS}_c$ is:

$$\overline{OS}_c \approx 2\,O/C - H/C \quad (8)$$

The $\overline{OS}_c$ of SOA from photooxidation of *m*-xylene/PAHs mixture increases from −0.54 to −0.37 for *m*-xylene/naphthalene, from −0.77 to 0.11 for *m*-xylene/1-methylnaphthalene, and from −0.41 to −0.43 for *m*-xylene/2-methylnaphthalene SOA. Kroll et al. (2011) reported that ambient organic aerosol $\overline{OS}_c$ values from −0.5 to 0 for SV-OOA and 0.5 to 0.9 for LV-OOA. Therefore, the PAH mixture SOA has similar $\overline{OS}_c$ to ambient SV-OOA, just as the SOA was consistent with the SV-OOA portion of triangle plot.

4. Conclusions

Previous studies have demonstrated that the SOA yield is potentially high for naphthalene and methylnaphthalenes photooxidation, and that the system reactivity (e.g., hydroxyl radical concentration, NO_x concentration) significantly impacts the SOA formed from these precursors. This study explores the SOA formation from PAHs mixed with either *m*-xylene or an atmospheric surrogate mixture during photooxidation under low NO_x conditions with and without H_2O_2. Traditional two-product models as well as m/z HR-ToF-AMS fragment analysis were applied to evaluate the aerosol mass contribution from individual PAH and *m*-xylene during PAH/*m*-xylene photooxidation. Our results indicated that SOA growth rate from PAH photooxidation was inhibited by *m*-xylene addition for low NO_x and H_2O_2 experiments, despite promoting earlier particles nucleation. Furthermore, the traditional two-product model using parameters derived from individual precursors over-predicted M_0 for *m*-xylene/PAHs photooxidation, suggesting that gas-phase cross-reaction chemistry or changes in the radical chemistry hinder the ability of the individual precursors to form SOA.

The SOA growth rate for different PAHs-*m*-xylene mixture was strongly correlated with initial $[HO_2]/[RO_2]$ ratio but negatively correlated with initial *m*-xylene/NO ratio, suggesting that the strong correlation is attributed to enhancement of SOA formation due to $HO_2 + RO_2$ chemistry, and the negative correlation is attributed to suppression of OH radical concentration due to *m*-xylene. The PAH-*m*-xylene mixture rapid conversion of NO to NO_2 greatly enhanced $HO_2 + RO_2$ reaction while the slow conversion of NO to NO_2 in individual PAH led to greater contribution of $RO_2 + NO$ chemistry. The reactivity changes in the systems by addition of species also alter the time of onset of SOA formation and hydrocarbon reacted. Only minimal changes in particle-phase bulk chemical composition was observed due to potential cross-reaction between the products from individual PAHs or *m*-xylene suggesting that additional cross reaction particle products were not strongly influencing SOA formation. However, the addition of *m*-xylene or atmospheric surrogate changes the gas-phase radical chemistry and influences the SOA formation from PAH precursor.

Acknowledgements

We gratefully acknowledge funding support from W.M. Keck Foundation and National Science Foundation (ATM-0449778 and ATM-0901282).

Appendix A. Supplementary data

Information details include supporting tables from Table S1 to S7 and figures from Fig. S1 to Fig. S13

The Supporting Information is available free of charge on the ACS Publications website at http://dx.doi.org/10.1016/j.atmosenv.2018.02.051.

References

Aiken, A.C., DeCarlo, P.F., Jimenez, J.L., 2007. Elemental analysis of organic species with electron ionization high-resolution mass spectrometry. Anal. Chem. 79, 8350–8358. http://dx.doi.org/10.1021/ac071150w.

Aiken, A.C., Decarlo, P.F., Kroll, J.H., Worsnop, D.R., Huffman, J.A., Docherty, K.S., Ulbrich, I.M., Mohr, C., Kimmel, J.R., Sueper, D., Sun, Y., Zhang, Q., Trimborn, A., Northway, M., Ziemann, P.J., Canagaratna, M.R., Onasch, T.B., Alfarra, M.R., Prevot, A.S.H., Dommen, J., Duplissy, J., Metzger, A., Baltensperger, U., Jimenez, J.L., 2008. O/C and OM/OC ratios of primary, secondary, and ambient organic aerosols with high-resolution time-of-flight aerosol mass spectrometry. Environ. Sci. Technol. 42, 4478–4485. http://dx.doi.org/10.1021/es703009q.

Alfarra, M.R., Coe, H., Allan, J.D., Bower, K.N., Boudries, H., Canagaratna, M.R., Jimenez, J.L., Jayne, J.T., Garforth, A.A., Li, S.M., Worsnop, D.R., 2004. Characterization of urban and rural organic particulate in the lower Fraser valley using two aerodyne aerosol mass spectrometers. Atmos. Environ. 38, 5745–5758. http://dx.doi.org/10.1016/j.atmosenv.2004.01.054.

Atkinson, R., Arey, J., 2007. Mechanisms of the gas-phase reactions of aromatic hydrocarbons and PAHs with OH and NO3 radicals. Polycycl. Aromat. Comp. 27, 15–40. http://dx.doi.org/10.1080/10406630601134243.

Bahreini, R., Keywood, M.D., Ng, N.L., Varutbangkul, V., Gao, S., Flagan, R.C., Seinfeld, J.H., Worsnop, D.R., Jimenez, J.L., 2005. Measurements of secondary organic aerosol from oxidation of cycloalkenes, terpenes, and m-xylene using an Aerodyne aerosol mass spectrometer. Environ. Sci. Technol. 39, 5674–5688. http://dx.doi.org/10.1021/es048061a.

Carter, W.P.L., Cocker, D.R., Fitz, D.R., Malkina, I.L., Bumiller, K., Sauer, C.G., Pisano, J.T., Bufalino, C., Song, C., 2005. A new environmental chamber for evaluation of gas-phase chemical mechanisms and secondary aerosol formation. Atmos. Environ. 39, 7768–7788. http://dx.doi.org/10.1016/j.atmosenv.2005.08.040.

Carter, W.P.L., 2010. Development of the SAPRC-07 chemical mechanism. Atmos. Environ. 44, 5324–5335. http://dx.doi.org/10.1016/j.atmosenv.2010.01.026.

Carter, W.P.L., Heo, G., 2013. Development of revised SAPRC aromatics mechanisms. Atmos. Environ. 77, 404–414. http://dx.doi.org/10.1016/j.atmosenv.2013.05.021.

Chan, M.N., Chan, A.W.H., Chhabra, P.S., Surratt, J.D., Seinfeld, J.H., 2009. Modeling of secondary organic aerosol yields from laboratory chamber data. Atmos. Chem. Phys. Discuss. 9 (2), 9457–9489. http://dx.doi.org/10.5194/acpd-9-9457-2009.

Chen, C.L., Kacarab, M., Tang, P., Cocker, D.R., 2016. SOA formation from naphthalene, 1-methylnaphthalene, and 2-methylnaphthalene photooxidation. Atmos. Environ. 131, 424–433. http://dx.doi.org/10.1016/j.atmosenv.2016.02.007.

Chhabra, P.S., Flagan, R.C., Seinfeld, J.H., 2010. Elemental analysis of chamber organic aerosol using an aerodyne high-resolution aerosol mass spectrometer. Atmos. Chem. Phys. 10, 4111–4131. http://dx.doi.org/10.5194/acp-10-4111-2010.

Chhabra, P.S., Ng, N.L., Canagaratna, M.R., Corrigan, A.L., Russell, L.M., Worsnop, D.R., Flagan, R.C., Seinfeld, J.H., 2011. Elemental composition and oxidation of chamber organic aerosol. Atmos. Chem. Phys. 11, 8827–8845. http://dx.doi.org/10.5194/acp-11-8827-2011.

Cocker, D.R., Flagan, R.C., Seinfeld, J.H., 2001 aa. State-of-the-art chamber facility for studying atmospheric aerosol chemistry. Environ. Sci. Technol. 35, 2594–2601. http://dx.doi.org/10.1021/es0019169.

Cocker, D.R., Mader, B.T., Kalberer, M., Flagan, R.C., Seinfeld, J.H., 2001 bb. The effect of

water on gas-particle partitioning of secondary organic aerosol: II. m-xylene and 1,3,5-trimethylbenzene photooxidation systems. Atmos. Environ. 35, 6073–6085. http://dx.doi.org/10.1016/s1352-2310(01)00405-8.
Conde, F.J., Ayala, J.H., Afonso, A.M., Gonzalez, V., 2005. Emissions of polycyclic aromatic hydrocarbons from combustion of agricultural and sylvicultural debris. Atmos. Environ. 39, 6654–6663. http://dx.doi.org/10.1016/j.atmosenv.2005.07.043.
de Gouw, J.A., Middlebrook, A.M., Warneke, C., Goldan, P.D., Kuster, W.C., Roberts, J.M., Fehsenfeld, F.C., Worsnop, D.R., Canagaratna, M.R., Pszenny, A.A.P., Keene, W.C., Marchewka, M., Bertman, S.B., Bates, T.S., 2005. Budget of organic carbon in a polluted atmosphere: results from the new england air quality study in 2002. J. Geophys. Res. Atmos. 110 (22). http://dx.doi.org/10.1029/2004jd005623.
DeCarlo, P.F., Kimmel, J.R., Trimborn, A., Northway, M.J., Jayne, J.T., Aiken, A.C., Gonin, M., Fuhrer, K., Horvath, T., Docherty, K.S., Worsnop, D.R., Jimenez, J.L., 2006. Field-deployable, high-resolution, time-of-flight aerosol mass spectrometer. Anal. Chem. 78, 8281–8289. http://dx.doi.org/10.1021/ac061249n.
Devore, J.L., Berk, K.N., 2012. Regression and Correlation. Springer New York, New York, NY, pp. 613–722.
Duplissy, J., DeCarlo, P.F., Dommen, J., Alfarra, M.R., Metzger, A., Barmpadimos, I., Prevot, A.S.H., Weingartner, E., Tritscher, T., Gysel, M., Aiken, A.C., Jimenez, J.L., Canagaratna, M.R., Worsnop, D.R., Collins, D.R., Tomlinson, J., Baltensperger, U., 2011. Relating hygroscopicity and composition of organic aerosol particulate matter. Atmos. Chem. Phys. 11, 1155–1165. http://dx.doi.org/10.5194/acp-11-1155-2011.
Forstner, H.J.L., Flagan, R.C., Seinfeld, J.H., 1997. Secondary organic aerosol from the photooxidation of aromatic hydrocarbons: molecular composition. Environ. Sci. Technol. 31, 1345–1358. http://dx.doi.org/10.1021/es9605376.
Heald, C.L., Jacob, D.J., Park, R.J., Russell, L.M., Huebert, B.J., Seinfeld, J.H., Liao, H., Weber, R.J., 2005. A large organic aerosol source in the free troposphere missing from current models. Geophys. Res. Lett. 32. http://dx.doi.org/10.1029/2005gl023831.
Heald, C.L., Kroll, J.H., Jimenez, J.L., Docherty, K.S., DeCarlo, P.F., Aiken, A.C., Chen, Q., Martin, S.T., Farmer, D.K., Artaxo, P., 2010. A simplified description of the evolution of organic aerosol composition in the atmosphere. Geophys. Res. Lett. 37 (5). http://dx.doi.org/10.1029/2010gl042737.
Hedberg, E., Kristensson, A., Ohlsson, M., Johansson, C., Johansson, P.A., Swietlicki, E., Vesely, V., Wideqvist, U., Westerholm, R., 2002. Chemical and physical characterization of emissions from birch wood combustion in a wood stove. Atmos. Environ. 36, 4823–4837. http://dx.doi.org/10.1016/s1352-2310(02)00417-x.
Henze, D.K., Seinfeld, J.H., Ng, N.L., Kroll, J.H., Fu, T.-M., Jacob, D.J., Heald, C.L., 2008. Global modeling of secondary organic aerosol formation from aromatic hydrocarbons: high- vs. low-yield pathways. Atmos. Chem. Phys. 8 (9), 2405–2420. http://dx.doi.org/10.5194/acp-8-2405-2008.
Hodzic, A., Jimenez, J.L., Madronich, S., Aiken, A.C., Bessagnet, B., Curci, G., Fast, J., Onasch, T.B., Roux, G., Ulbrich, I.M., 2009. Modeling organic aerosols during MILAGRO: importance of biogenic secondary organic aerosols. Geochem. Cosmochim. Acta 73 A537–A537.
Izumi, K., Fukuyama, T., 1990. Photochemical aerosol formation from aromatic-hydrocarbons in the presence of NOX. Atmos. Environ. Part a-General Topics 24, 1433–1441. http://dx.doi.org/10.1016/0960-1686(90)90052-o.
Kautzman, K.E., Surratt, J.D., Chan, M.N., Chan, A.W.H., Hersey, S.P., Chhabra, P.S., Dalleska, N.F., Wennberg, P.O., Flagan, R.C., Seinfeld, J.H., 2010. Chemical composition of gas- and aerosol-phase products from the photooxidation of naphthalene. J. Phys. Chem. 114, 913–934. http://dx.doi.org/10.1021/jp908530s.
Kleinman, L.I., Springston, S.R., Daum, P.H., Lee, Y.N., Nunnermacker, L.J., Senum, G.I., Wang, J., Weinstein-Lloyd, J., Alexander, M.L., Hubbe, J., Ortega, J., Canagaratna, M.R., Jayne, J., 2008. The time evolution of aerosol composition over the Mexico City plateau. Atmos. Chem. Phys. 8, 1559–1575. http://dx.doi.org/10.5194/acp-8-1559-2008.
Kroll, J.H., Ng, N.L., Murphy, S.M., Flagan, R.C., Seinfeld, J.H., 2006. Secondary organic aerosol formation from isoprene photooxidation. Environ. Sci. Technol. 40, 1869–1877. http://dx.doi.org/10.1021/es0524301.
Kroll, J.H., Donahue, N.M., Jimenez, J.L., Kessler, S.H., Canagaratna, M.R., Wilson, K.R., Altieri, K.E., Mazzoleni, L.R., Wozniak, A.S., Bluhm, H., Mysak, E.R., Smith, J.D., Kolb, C.E., Worsnop, D.R., 2011. Carbon oxidation state as a metric for describing the chemistry of atmospheric organic aerosol. Nat. Chem. 3, 133–139. http://dx.doi.org/10.1038/nchem.948.
Li, L., Tang, P., Nakao, S., Chen, C.L., Cocker, D.R., 2016. Role of methyl group number on SOA formation from monocyclic aromatic hydrocarbons photooxidation under low-NOx conditions. Atmos. Chem. Phys. 16, 2255–2272. http://dx.doi.org/10.5194/acp-16-2255-2016.
Li, L.J., Tang, P., Cocker, D.R., 2015. Instantaneous nitric oxide effect on secondary organic aerosol formation from m-xylene photooxidation. Atmos. Environ. 119, 144–155. http://dx.doi.org/10.1016/j.atmosenv.2015.08.010.
Li, L.J., Qi, L., Cocker, D.R., 2017. Contribution of methyl group to secondary organic aerosol formation from aromatic hydrocarbon photooxidation. Atmos. Environ. 151, 133–139. http://dx.doi.org/10.1016/j.atmosenv.2016.11.064.
Li, W., Li, L., Chen, C., Kacarab, M., Peng, W., Price, D., Xu, J., Cocker, D.R., 2018. Potential of select intermediate-volatility organic compounds and consumer products for secondary organic aerosol and ozone formation under relevant urban conditions. Atmos. Environ. 178, 109–117. http://dx.doi.org/10.1016/j.atmosenv.2017.12.019.
Loza, C.L., Chhabra, P.S., Yee, L.D., Craven, J.S., Flagan, R.C., Seinfeld, J.H., 2012. Chemical aging of m-xylene secondary organic aerosol: laboratory chamber study. Atmos. Chem. Phys. 12, 151–167. http://dx.doi.org/10.5194/acp-12-151-2012.
Malloy, Q.G.J., Nakao, S., Qi, L., Austin, R., Stothers, C., Hagino, H., Cocker, D.R., 2009. Real-time aerosol density determination utilizing a modified scanning mobility particle SizerAerosol particle mass analyzer system. Aerosol. Sci. Technol. 43, 673–678. http://dx.doi.org/10.1080/02786820902832960.
McDonald, J.D., Zielinska, B., Fujita, E.M., Sagebiel, J.C., Chow, J.C., Watson, J.G., 2003. Emissions from charbroiling and grilling of chicken and beef. J. Air Waste Manag. Assoc. 53, 185–194.
Nakao, S., Clark, C., Tang, P., Sato, K., Cocker, D., 2011 aa. Secondary organic aerosol formation from phenolic compounds in the absence of NOx. Atmos. Chem. Phys. 11, 10649–10660. http://dx.doi.org/10.5194/acp-11-10649-2011.
Nakao, S., Shrivastava, M., Nguyen, A., Jung, H.J., Cocker, D., 2011 bb. Interpretation of secondary organic aerosol formation from diesel exhaust photooxidation in an environmental chamber. Aerosol. Sci. Technol. 45 (9). http://dx.doi.org/10.1080/02786826.2011.573510.
Nakao, S., Liu, Y., Tang, P., Chen, C.L., Zhang, J., Cocker, D.R., 2012. Chamber studies of SOA formation from aromatic hydrocarbons: observation of limited glyoxal uptake. Atmos. Chem. Phys. 12, 3927–3937. http://dx.doi.org/10.5194/acp-12-3927-2012.
Ng, N.L., Kroll, J.H., Chan, A.W.H., Chhabra, P.S., Flagan, R.C., Seinfeld, J.H., 2007. Secondary organic aerosol formation from m-xylene, toluene, and benzene. Atmos. Chem. Phys. 7, 3909–3922.
Ng, N.L., Canagaratna, M.R., Zhang, Q., Jimenez, J.L., Tian, J., Ulbrich, I.M., Kroll, J.H., Docherty, K.S., Chhabra, P.S., Bahreini, R., Murphy, S.M., Seinfeld, J.H., Hildebrandt, L., Donahue, N.M., DeCarlo, P.F., Lanz, V.A., Prevot, A.S.H., Dinar, E., Rudich, Y., Worsnop, D.R., 2010. Organic aerosol components observed in Northern Hemispheric datasets from aerosol mass spectrometry. Atmos. Chem. Phys. 10, 4625–4641. http://dx.doi.org/10.5194/acp-10-4625-2010.
Nishino, N., Arey, J., Atkinson, R., 2009. Yields of glyoxal and ring-cleavage Co-Products from the OH radical-initiated reactions of naphthalene and selected alkylnaphthalenes. Environ. Sci. Technol. 43, 8554–8560. http://dx.doi.org/10.1021/es902018v.
Nishino, N., Arey, J., Atkinson, R., 2012. 2-Formylcinnamaldehyde formation yield from the OH radical-initiated reaction of naphthalene: effect of NO2 concentration. Environ. Sci. Technol. 46, 8198–8204. http://dx.doi.org/10.1021/es301865t.
Odum, J.R., Hoffmann, T., Bowman, F., Collins, D., Flagan, R.C., Seinfeld, J.H., 1996. Gas/particle partitioning and secondary organic aerosol yields. Environ. Sci. Technol. 30, 2580–2585. http://dx.doi.org/10.1021/es950943+.
Odum, J.R., Jungkamp, T.P.W., Griffin, R.J., Forstner, H.J.L., Flagan, R.C., Seinfeld, J.H., 1997. Aromatics, reformulated gasoline, and atmospheric organic aerosol formation. Environ. Sci. Technol. 31, 1890–1897. http://dx.doi.org/10.1021/es960535l.
Qi, L., Nakao, S., Malloy, Q., Warren, B., Cocker, D.R., 2010. Can secondary organic aerosol formed in an atmospheric simulation chamber continuously age? Atmos. Environ. 44, 2990–2996. http://dx.doi.org/10.1016/j.atmosenv.2010.05.020.
Sato, K., Takami, A., Isozaki, T., Hikida, T., Shimono, A., Imamura, T., 2010. Mass spectrometric study of secondary organic aerosol formed from the photo-oxidation of aromatic hydrocarbons. Atmos. Environ. 44, 1080–1087. http://dx.doi.org/10.1016/j.atmosenv.2009.12.013.
Schwier, A.N., Sareen, N., Mitroo, D., Shapiro, E.L., McNeill, V.F., 2010. Glyoxal-methylglyoxal cross-reactions in secondary organic aerosol formation. Environ. Sci. Technol. 44, 6174–6182. http://dx.doi.org/10.1021/es101225q.
Shah, S.D., Ogunyoku, T.A., Miller, J.W., Cocker, D.R., 2005. On-road emission rates of PAH and n-alkane compounds from heavy-duty diesel vehicles. Environ. Sci. Technol. 39, 5276–5284. http://dx.doi.org/10.1021/es048086+.
Shakya, K.M., Griffin, R.J., 2010. Secondary organic aerosol from photooxidation of polycyclic aromatic hydrocarbons. Environ. Sci. Technol. 44, 8134–8139. http://dx.doi.org/10.1021/es1019417.
Song, C., Na, K.S., Cocker, D.R., 2005. Impact of the hydrocarbon to NOx ratio on secondary organic aerosol formation. Environ. Sci. Technol. 39, 3143–3149. http://dx.doi.org/10.1021/es0493244.
Song, C., Na, K., Warren, B., Malloy, Q., Cocker, D.R., 2007. Secondary organic aerosol formation from m-xylene in the absence of NOx. Environ. Sci. Technol. 41, 7409–7416. http://dx.doi.org/10.1021/es070429r.
Takekawa, H., Minoura, H., Yamazaki, S., 2003. Temperature dependence of secondary organic aerosol formation by photo-oxidation of hydrocarbons. Atmos. Environ. 37, 3413–3424. http://dx.doi.org/10.1016/s1352-2310(03)00359-5.
Utembe, S.R., Cooke, M.C., Archibald, A.T., Shallcross, D.E., Derwent, R.G., Jenkin, M.E., 2011. Simulating secondary organic aerosol in a 3-D Lagrangian chemistry transport model using the reduced Common Representative Intermediates mechanism (CRI v2-R5). Atmos. Environ. 45, 1604–1614. http://dx.doi.org/10.1016/j.atmosenv.2010.11.046.
Volkamer, R., Jimenez, J.L., San Martini, F., Dzepina, K., Zhang, Q., Salcedo, D., Molina, L.T., Worsnop, D.R., Molina, M.J., 2006. Secondary organic aerosol formation from anthropogenic air pollution: rapid and higher than expected. Geophys. Res. Lett. 33 (4). http://dx.doi.org/10.1029/2006gl026899.
Wang, L., Atkinson, R., Arey, J., 2007. Dicarbonyl products of the OH radical-initiated reactions of naphthalene and the C-1- and C-2-alkylnaphthalenes. Environ. Sci. Technol. 41, 2803–2810. http://dx.doi.org/10.1021/es0628102.
Zhang, Q., Jimenez, J.L., Canagaratna, M.R., Allan, J.D., Coe, H., Ulbrich, I., Alfarra, M.R., Takami, A., Middlebrook, A.M., Sun, Y.L., Dzepina, K., Dunlea, E., Docherty, K., DeCarlo, P.F., Salcedo, D., Onasch, T., Jayne, J.T., Miyoshi, T., Shimono, A., Hatakeyama, S., Takegawa, N., Kondo, Y., Schneider, J., Drewnick, F., Borrmann, S., Weimer, S., Demerjian, K., Williams, P., Bower, K., Bahreini, R., Cottrell, L., Griffin, R.J., Rautiainen, J., Sun, J.Y., Zhang, Y.M., Worsnop, D.R., 2007. Ubiquity and dominance of oxygenated species in organic aerosols in anthropogenically-influenced Northern Hemisphere midlatitudes. Geophys. Res. Lett. 34 (6). http://dx.doi.org/10.1029/2007gl029979.
Zhang, Y., Liu, P., Queen, A., Misenis, C., Pun, B., Seigneur, C., Wu, S.Y., 2006. A comprehensive performance evaluation of MM5-CMAQ for the Summer 1999 Southern Oxidants Study episode- Part II: Gas and aerosol predictions. Atmos. Environ. 40, 4839–4855. http://dx.doi.org/10.1016/j.atmonsenv.2005.12.048.